

**From Precipitation to Prediction: Using ConvLSTM  
Models for Comprehensive River Runoff Forecasting**

**Florian Börgel<sup>1</sup>, Sven Karsten<sup>1</sup>, Karoline Rummel<sup>1</sup>**

<sup>1</sup>Leibniz-Institute for Baltic Sea Research Warnemünde,

5      **Abstract**  
 6      a

7      **Plain Language Summary**  
 8      b

9      **1 Introduction**

10     River runoff is an important component of the global water cycle as it comprises  
 11    about one third of the precipitation over land areas (Hagemann et al., 2020). Therefore,  
 12    accurate runoff forecasting is crucial for effective water resources management,  
 13    particularly over extended periods (Fang et al., 2019; Tan et al., 2018). In the context  
 14    of climate change studies, river runoff is usually generated in two ways. First,  
 15    river runoff as input for ocean models can be created using hydrological models such  
 16    as the Hydrological Discharge (HD) model (Hagemann et al., 2020). HD models  
 17    calculate the water balance using hydrological processes (e.g. snow, glaciers, soil  
 18    moisture, groundwater contribution). It represents a complex forecasting tool that  
 19    uses underlying physical processes. The second approach uses data-driven models  
 20    that integrate statistical correction, using land surface schemes of global or regional  
 21    climate models [QUELLE].

22     With the recent rise of machine learning in climate research various model archi-  
 23    tectures have also been tested for river runoff forecasting. Common approaches  
 24    employ feed-forward artificial neural networks, support vector machines, adaptive  
 25    neuro-fuzzy inference systems, and notably, Long Short-Term Memory (LSTM) neu-  
 26    ral networks that have gained traction for long-term hydrological forecasting due  
 27    to their excellent performance (**humphrey2016hybrid?**; **huang2014monthly?**;  
 28    **ashrafi2017fully?**; **liu2020streamflow?**; **fang2022application?**; **kratzert2018rainfall?**).

29     LSTM networks, first introduced by (**hochreiter1997long?**) , are an evolution  
 30    of the classical Recurrent Neural Networks (RNNs). Their structure enables them  
 31    to learn long-term dependencies while avoiding the vanishing or exploding gra-  
 32    dient problem. They have shown stability and efficacy in sequence-to-sequence  
 33    predictions. However, a limitation of LSTMs is their inability to effectively cap-  
 34    ture two-dimensional structures, an area where Convolutional Neural Networks  
 35    (CNNs) excel. Recognizing this limitation SHI et al. (2015) proposed a Convolu-  
 36    tional LSTM (ConvLSTM) architecture, which combines the strengths of both  
 37    LSTM and CNN. The ConvLSTM network has been proven useful for spatio-  
 38    temporal applications such as precipitation nowcasting (SHI et al., 2015), flood  
 39    forecasting (**moishin2021designing?**), and river runoff forecasting (**ha2021?**;  
 40    **zhu2023spatiotemporal?**).

41     In this work, we demonstrate that ConvLSTM networks are a reliable method for  
 42    predicting multiple rivers simultaneously, using only atmospheric forcing, even in the  
 43    absence of a fully functional hydrological model with a complex parameterization.  
 44    We use the Baltic Sea catchment as an example to illustrate our approach. Although  
 45    the methodology we propose is universally applicable across various geographic re-  
 46    gions, the Baltic Sea represents a challenging region due to its unique hydrological  
 47    characteristics, being nearly decoupled from the open ocean (see Figure). As a con-  
 48    sequence, the salinity of the Baltic Sea is driven to a large part by freshwater supply  
 49    from rivers. Freshwater enters the Baltic Sea through river runoff or positive net  
 50    precipitation (precipitation minus evaporation) over the sea surface. The net precip-  
 51    itation accounts for 11 % and the river input for 89 % of the total freshwater input  
 52    (**meier2002simulated?**). Modelling the Baltic Sea is therefore to a large part the  
 53    result of the quality of the river input, that is used for the simulation. This makes  
 54    the accurate modeling of river runoff especially critical for simulations pertaining to  
 55    the Baltic Sea.

56 In this work we will, we present a ConvLSTM architecture that is able to predict  
 57 daily river runoff for 97 rivers across the Baltic Sea catchment. ***mehr Fokus auf***  
 58 ***Neues?***

## 59 **2 Implemented model architecture**

### 60 **2.1 The main idea**

61 We assume that the runoff at a specific point in time for all  $N_r$  considered rivers,  
 62 collected in the vector  $\vec{R}^t \in \mathbb{R}^{N_r}$ , can be accurately approximated by a functional  
 63  $\vec{M}(\{X_k^t[x, y, \tau]\})$  of  $k = 1, \dots, N_k$  atmospheric fields  $X_k^t[x, y, \tau]$  which are known for  
 64 the past  $\tau = 1, \dots, N_\tau$  time instances. This relationship is expressed as:

$$\vec{R}^t = \vec{M}(\{X_k^t[x, y, \tau]\}).$$

65 The atmospheric fields are evaluated over a spatial domain  $x = 1, \dots, N_x$  and  
 66  $y = 1, \dots, N_y$  which is sufficiently large to capture all significant local and non-local  
 67 contributions of the atmospheric fields to the river runoff.

68 Typically, such a mapping is realized using a hydrological model that simulates all  
 69 relevant physical processes, transforming variables like precipitation and evapora-  
 70 tion into river runoff. This process relies heavily on domain knowledge to tune all  
 71 parameters to reasonable values.

72 As an alternative, we propose that this functional can be adequately represented by  
 73 a combination of a convolutional Long-Short Term Memory (ConvLSTM) model  
 74 with a subsequent fully connected neural network. This approach eliminates the  
 75 need for detailed knowledge of the involved processes and their modeling. Instead,  
 76 these features can be “learned” by the network in an automated manner. Our pro-  
 77 posed network architecture is visualized in Figure 1 and described in detail in the  
 78 following sections. To provide an overview, we will discuss the main components of  
 79 this architecture one-by-one.

### 80 **2.2 ConvLSTM network**

#### 81 **2.2.1 The LSTM approach**

82 Before turning directly to the ConvLSTM the simpler architecture of the plain Long-  
 83 Short Term Memory (LSTM) model is examined which serves as a foundation for  
 84 understanding the more complex ConvLSTM.

85 The LSTM, a specialized form of Recurrent Neural Networks (RNNs), is specifically  
 86 designed to model temporal sequences  $\vec{X}^t[1], \dots, \vec{X}^t[\tau], \dots, \vec{X}^t[N_\tau]$  of  $N_\tau$  input quanti-  
 87 ties  $\vec{X}^t[\tau] = (X_k^t[\tau]) \in \mathbb{R}^{N_k}$ . This sequence is taken from a dataset given in form of  
 88 a time series  $\{\vec{X}^t\}$  with the endpoint coinciding with the specific element in the time  
 89 series connected to time  $t$ , i.e.  $\vec{X}^t[N_\tau] \equiv \vec{X}^t$ , see Figure 1. Here,  $N_k$  represents the  
 90 number of input “channels,” which can correspond to different measurable quanti-  
 91 ties. The LSTM’s unique design allows it to adeptly handle long-range dependencies,  
 92 setting it apart from traditional RNNs in terms of accuracy (see Figure 2).

93 This performance in modeling long-range dependencies has been validated in var-  
 94 ious studies (**XXX?**). The key component of the LSTM’s innovation is its cell  
 95 state,  $\vec{C}^t[\tau] = (C_h^t[\tau]) \in \mathbb{R}^{N_h}$ , which stores state information, also referred to as  
 96 *long-term memory*. This state information complements the so-called hidden state  
 97  $\vec{H}^t[\tau] = (H_h^t[\tau]) \in \mathbb{R}^{N_h}$  vector, which is also known from simpler neural network  
 98 architectures. In case of the LSTM, the hidden state vector plays the role of the  
 99 *short-term memory*.

100 A significant advantage of this architecture is the memory cell’s ability to retain gra-  
 101 dients. This mechanism addresses the vanishing gradient problem, where, as input  
 102 sequences elongate, the influence of initial stages becomes harder to capture, causing  
 103 gradients of early input points to approach zero. The LSTM’s activation function,

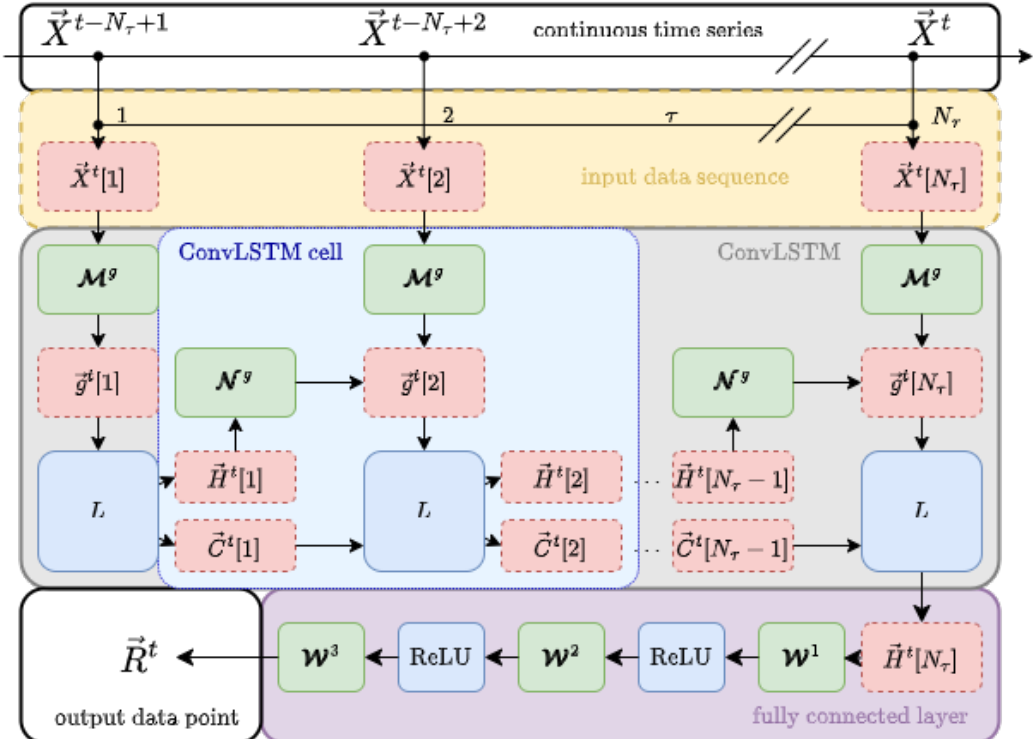


Figure 1: **Combined ConvLSTM and FC network architecture.** The starting point is the continuous timeseries of input data  $\{\vec{X}^t\}$ , upper white block. From this series, a contiguous sequence of  $N_\tau$  elements (yellow block) is used to feed a chain of  $N_\tau$  connected ConvLSTM cells (light blue block) building the ConvLSTM network (grey block). The input sequence is mapped via weighting matrices  $\mathcal{M}^g$  (green blocks) onto gate vectors  $\vec{g}^t[\tau]$ . The gate vectors are then used to update the cell state  $\vec{C}^t[\tau - 1]$  and the hidden state  $\vec{H}^t[\tau - 1]$  of the last ConvLSTM cell to the current values  $\vec{C}^t[\tau]$  and  $\vec{H}^t[\tau]$ , respectively. The update is performed with LSTM core equations collectively described by the mapping  $L$ , see Equation 2. The weighting matrices  $\mathcal{N}^g$  (green blocks) control how much of the last hidden state enters the updated state. The final output of the ConvLSTM  $\vec{H}^t[\tau]$  is then propagated to a FC network, which itself is a chain of three FC layers consisting of weighting matrices  $\mathbf{W}$  and connected via ReLU functions, see Section 2.3. The final result is then the river runoff  $\vec{R}^t$  for all rivers considered at the current time instance  $t$  (white block on the lower left). Note that all bias vectors are omitted for the sake of clarity. See text for more information.

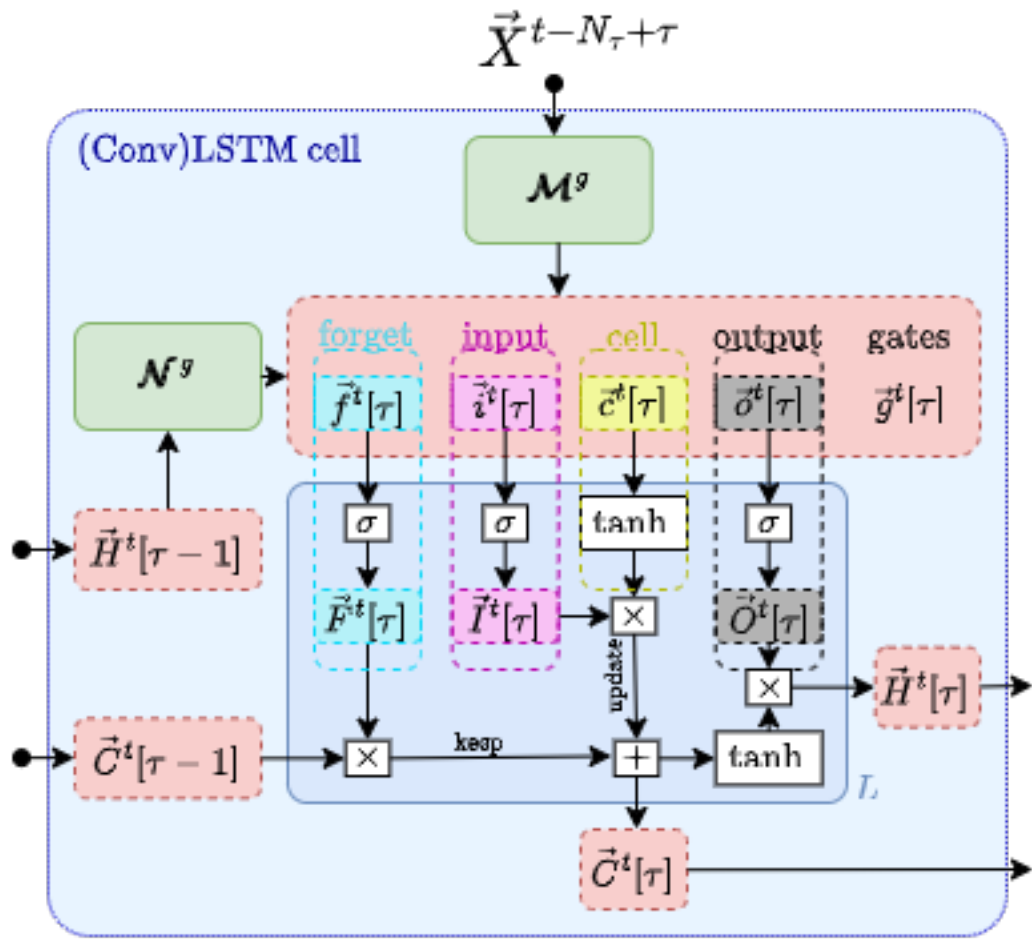


Figure 2: **Inner structure of a Long Short-Term Memory Cell.** See Figure 1 and text for information.

104 inherently recurrent, mirrors the identity function with a consistent derivative of 1.0,  
 105 ensuring the gradient remains stable throughout backpropagation.

106 The cell state and the hidden state are vectors, where each element is associated  
 107 with one of the  $N_h$  hidden layers, labeled by  $h$ , which are internal, *artificial* degrees  
 108 of freedom that enable the high adaptability of neural networks. These two state vec-  
 109 tors are determined through several self-parameterized gates, all in the same vector  
 110 space as  $\vec{C}^t[\tau]$ , see Figure 2 for a visualization.

111 In particular, the forget gate  $\vec{F}^t[\tau]$  defines the portion of the previous (long-term  
 112 memory) cell state  $\vec{C}^t[\tau - 1]$  that should be kept, see dashed cyan box therein. The  
 113 input gate  $\vec{I}^t[\tau]$  controls the contribution of the current input used to update the  
 114 long-term memory,  $\vec{C}^t[\tau]$  (magenta and yellow boxes). The output gate,  $\vec{O}^t[\tau]$ , then  
 115 determines how much of this updated long-term memory contributes to the new  
 116 (short-term memory) hidden state,  $\vec{H}^t[\tau]$  (black dashed box).

117 For a fixed point  $\tau$  in the sequence, the action of a LSTM cell, i.e. the connection  
 118 between the input  $\vec{X}^t[\tau]$ , the various gates and the state vectors, is mathematically  
 119 given as follows.

120 First, the elements of the input sequence together with the hidden state are mapped  
 121 onto auxiliary gate vectors, collectively denoted by  $\vec{g}^t[\tau] = (g_h^t[\tau]) \in \mathbb{R}^{N_h}$ , via

$$g_h^t[\tau] = \mathcal{M}_{hk}^g X_k^t[\tau] + \mathcal{N}_{hh'}^g H_{h'}^t[\tau - 1] + \mathcal{B}_h^g ,$$

122 where  $g = i, f, o, c$  stands for the input, forget, output and cell-state gate, respec-  
 123 tively and Einstein's summation convention is employed, i.e. indices that appear  
 124 twice are summed over. The calligraphic symbols  $\mathcal{M}_{hk}^g$ ,  $\mathcal{N}_{hh'}^g$  and  $\mathcal{B}_h^g$  are the free  
 125 parameters of the network that are optimized for the given problem during the  
 126 training, which is at the heart of any machine learning approach. The matrix  
 127  $\mathcal{M}^g = (\mathcal{M}_{hk}^g) \in \mathbb{R}^{N_h \times N_k}$  can be interpreted as a Markovian-like contribution of  
 128 the current input  $\vec{X}^t[\tau]$  to the gates, whereas the  $\mathcal{N}^g = (\mathcal{N}_{hh'}^g) \in \mathbb{R}^{N_h \times N_h}$  scales a  
 129 non-Markovian part determined by the hidden state of the last sequence point  $\tau - 1$ .  
 130 The vector  $\mathcal{B}^g = (\mathcal{B}_h^g) \in \mathbb{R}^{N_h}$  is a learnable bias. It should be stressed that these  
 131 parameters do neither depend on  $t$  nor on  $\tau$  and are thus optimized once for the  
 132 complete dataset  $\{\vec{X}^t\}$ .

133 Note that this mapping is sometimes extended by a contribution to the  $g_h^t[\tau]$  from  
 134 the past cell state  $\vec{C}^t[\tau - 1]$  (**XXX?**). Nevertheless, this mechanism called “peeping”  
 135 is not further considered in this work.

136 For the sake of brevity, we can write the mapping more compactly in matrix-vector  
 137 form as

$$\vec{g}^t[\tau] = \mathcal{M}^g \vec{X}^t[\tau] + \mathcal{N}^g \vec{H}^t[\tau - 1] + \vec{\mathcal{B}}^g \quad (1)$$

138 Second, the actual gate vectors are computed by the core equations of the LSTM as  
 139 proposed by (**hochreiter1997long?**):

$$\begin{aligned} \vec{I}^t[\tau] &= \sigma(\vec{i}^t[\tau]) \\ \vec{F}^t[\tau] &= \sigma(\vec{f}^t[\tau]) \\ \vec{O}^t[\tau] &= \sigma(\vec{o}^t[\tau]) \\ \vec{C}^t[\tau] &= \vec{F}^t[\tau] \circ \vec{C}^t[\tau - 1] + \vec{I}^t[\tau] \circ \tanh(\vec{c}^t[\tau]) \\ \vec{H}^t[\tau] &= \vec{O}^t[\tau] \circ \tanh(\vec{C}^t[\tau]) , \end{aligned} \quad (2)$$

140 where  $\sigma$  denotes the logistic sigmoid function,  $\tanh$  is the hyperbolic tangent and  
 141 the  $\circ$  stands for the Hadamard product (all applied in an element-wise fashion to the

vectors). In the last two equations the role of the input, forget and output gates as described above becomes apparent.

The third step in a single layer LSTM (as employed for the work presented here) is then to provide the output of the current LSTM cell, i.e.  $\vec{H}^t[\tau]$  and  $\vec{C}^t[\tau]$ , to the subsequent LSTM cell that processes the next element  $\vec{X}^t[\tau + 1]$  of the input sequence.

The full action of the LSTM network up to the end of the sequence can be written as a nested function call

$$(\vec{H}^t[N_\tau], \vec{C}^t[N_\tau]) = L(\vec{X}^t[N_\tau], L(\vec{X}^t[N_\tau - 1], \dots L(\vec{X}^t[1], (\vec{H}^t[0], \vec{C}^t[0])) \dots)) , \quad (3)$$

where  $L(\vec{X}^t[\tau], (\vec{H}^t[\tau - 1], \vec{C}^t[\tau - 1]))$  represents Equation 1 and Equation 2. For the present work, the initial conditions are chosen as  $\vec{H}^t[0] = \vec{C}^t[0] = 0$ , which simply means that there is no memory longer than  $N_\tau$  time steps.

The final output of the ConvLSTM chain,  $\vec{H}^t[N_\tau]$  and  $\vec{C}^t[N_\tau]$ , encode information on the full input sequence ending at time  $t$ . This information has to be decoded to obtain useful information via an appropriate subsequent network, as it is described in the Section 2.3.

### 2.2.2 Combining LSTM with spatial convolution

Although the plain LSTM has high performance in handling temporal sequences of point-like quantities it is not designed to recognize spatial features in sequences of, e.g., two-dimensional maps as atmospheric-ocean interface fields. To address this limitation we employ a ConvLSTM architecture as described in the following.

In this kind of network the elements of the input sequence are given as spatially varying fields  $\vec{X}^t[\tau] = (X_k^t[x, y, \tau]) \in \mathbb{R}^{N_k \times (N_x \times N_y)}$ , where  $x \in [1, N_x]$  and  $y \in [1, N_y]$  run over the horizontal and vertical dimensions of the map, respectively. In order to enable the “learning” of spatial patterns, the free parameters of the network are replaced by two-dimensional convolution kernels  $\mathcal{M}^g = (\mathcal{M}_{hk}^g[\xi, \eta]) \in \mathbb{R}^{(N_h \times N_k) \times (N_\xi \times N_\eta)}$  and  $\mathcal{N}^g = (\mathcal{N}_{hh'}^g[\xi, \eta]) \in \mathbb{R}^{(N_h \times N_h) \times (N_\xi \times N_\eta)}$ . The width and the height of the kernels are given by  $N_\xi$  and  $N_\eta$ , respectively and  $\xi \in [-(N_\xi - 1)/2, (N_\xi - 1)/2]$ ,  $\eta \in [-(N_\eta - 1)/2, (N_\eta - 1)/2]$ , where, without loss of generality, we assume odd numbers for the kernel sizes.

The mapping from the input quantities to the gates is then given by a convolution with these kernels

$$g_h^t[x, y, \tau] = \mathcal{M}_{hk}^g[\xi, \eta] X_k^t[x - \xi, y - \eta, \tau] + \mathcal{N}_{hh'}^g[\xi, \eta] H_{h'}^t[x - \xi, y - \eta, \tau - 1] + \mathcal{B}_h^g .$$

again with Einstein’s convention imposed.

It becomes immediately apparent that in case of the ConvLSTM, the gate and state vectors must become vector fields ( $\in \mathbb{R}^{N_h \times (N_x \times N_y)}$ ) as well. We can write this mapping in the same way as Equation 1 but with replacing the normal matrix-vector multiplication by a convolution (denoted with  $*$ ), i.e.

$$\vec{g}^t[\tau] = \mathcal{M}^g * \vec{X}^t[\tau] + \mathcal{N}^g * \vec{H}^t[\tau - 1] + \vec{\mathcal{B}}^g$$

The subsequent processing of the  $\vec{g}^t[\tau]$  remains symbolically the same as presented in Equation 2 but with all appearing quantities now meaning vector fields instead of simple vectors.

In summary, the ConvLSTM excels at processing tasks that demand a combined understanding of spatial patterns and temporal sequences in data. It merges the image-processing capabilities of Convolutional Neural Networks (CNNs) with the time-series modeling of Long Short-Term Memory (LSTM) networks.

185 **2.3 Fully connected layer**

186 As stated in Sec. Section 2.2.1, the final output  $\vec{H}^t[N_\tau]$  and  $\vec{C}^t[N_\tau]$  of the Con-  
 187 vLSTM encode information on the full input sequence. In order to contract this  
 188 information to obtain the runoff vector  $\vec{R}^t$  representing the  $N_r$  rivers, we propose to  
 189 subject the final short-term memory (i.e. the hidden state  $\vec{H}^t[N_\tau]$ ) to an additional  
 190 FC network.

191 In particular, the dimensionality of the vector field  $\vec{H}^t[N_\tau]$  is sequentially reduced  
 192 by three nested FC layers, each connected to the other by the Rectified Linear Unit  
 193 (ReLU), see Figure 1. Integrating over artificial degrees of freedom in a step-wise  
 194 fashion has turned out to be benificial [(**XXX?**)].

195 Spelled out in mathematics, the runoff of the  $r$ -th river is then obtained via (using  
 196 Einstein's convention)

$$R_r^t = \mathcal{W}_{rb}^3 \text{ReLU} (\mathcal{W}_{ba}^2 \text{ReLU} (\mathcal{W}_{ah}^1 [x, y] H_h^t [x, y, N_\tau] + \mathcal{B}_a^1) + \mathcal{B}_b^2) + \mathcal{B}_r^3 ,$$

197 where  $a = 1, \dots, N_a$ ,  $b = 1, \dots, N_b$  and the hyper parameters  $N_a$  and  $N_b$  are chosen  
 198 such that  $N_h \cdot N_x \cdot N_y > N_a > N_b > N_r$  in order to achieve the aforementioned  
 199 step-by-step reduction of dimensionality. The weights  $\mathcal{W}$  and biases  $\mathcal{B}$  stand for  
 200 parameters that are optimized during the training of the network.

201 In matrix-vector notation this can be compactified to

$$\vec{R}^t = \mathcal{W}^3 \text{ReLU} (\mathcal{W}^2 \text{ReLU} (\mathcal{W}^1 \vec{H}^t [N_\tau] + \vec{\mathcal{B}}^1) + \vec{\mathcal{B}}^2) + \vec{\mathcal{B}}^3 .$$

202 Combining the last equation with Equation 3 provides finally an explicit formula for  
 203 the initial assumption of modelling the runoff for time  $t$  as a functional of a sequence  
 204 of atmospheric fields, i.e.

$$\begin{aligned} \vec{R}^t &= \vec{M}(\{X_k^t [x, y, \tau]\}) \\ &= \mathcal{W}^3 \text{ReLU} (\mathcal{W}^2 \text{ReLU} (\mathcal{W}^1 \vec{L}_H (\vec{X}^t [N_\tau], L(\vec{X}^t [N_\tau - 1], \dots, L(\vec{X}^t [1], (0, 0)) \dots)) + \vec{\mathcal{B}}^1) + \vec{\mathcal{B}}^2) + \vec{\mathcal{B}}^3 , \end{aligned}$$

205 where the  $\vec{L}_H$  means that only the hidden state vector of the final ConvLSTM call is  
 206 forwarded to the FC layer.

207 In Section 3, we present the employed model and data setup as well as the choice for  
 208 all mentioned hyper parameters that lead to an adequate model performance after  
 209 training.

210 **3 Technical details**

211 **3.1 Runoff data used for training**

212 The runoff data covering the period 1979 to 2011 is based on an E-HYPE hindcast  
 213 simulation that was forced by a regional downscaling of ERA-Interim (**dee2011?**)  
 214 with RCA3 (**theross?**) and implemented into NEMO-Nordic (**hordoir2019?**) as a  
 215 mass flux. For the periods before (1961 to 1978) and after (2012 to 2018) additional  
 216 spatial temporal corrections have been applied to the runoff data, and have there-  
 217 fore been ignored. The quality of the runoff was extensively evaluated. For more  
 218 information see (**gröger2022?**) and references therein.

219 **3.2 Atmospheric Forcing**

220 The UERRA-HARMONIE regional reanalysis dataset was developed as part of  
 221 the FP7 UERRA project (Uncertainties in Ensembles of Regional Re-Analyses,  
 222 <http://www.uerra.eu/>). The UERRA-HARMONIE system represents a comprehen-  
 223 sive, high-resolution reanalysis covering a wide range of essential climate variables.  
 224 This dataset encompasses data on air temperature, pressure, humidity, wind speed

and direction, cloud cover, precipitation, albedo, surface heat fluxes, and radiation fluxes from January 1961 to July 2019. With a horizontal resolution of 11 km and analyses conducted at 00 UTC, 06 UTC, 12 UTC, and 18 UTC, it also provides hourly resolution forecast model data. UERRA-HARMONIE is accessible through the Copernicus Climate Data Store (CDS, <https://cds.climate.copernicus.eu/#!/home>), initially produced during the UERRA project and later transitioned to the Copernicus Climate Change Service (C3S, <https://climate.copernicus.eu/copernicus-regionalreanalysis-europe>).

### 3.3 Ocean Model

To simulate the Baltic Sea, we use a coupled 3-dimensional ocean model Baltic Sea, called the Modular Ocean Model (MOM). This model uses a finite-difference method to solve the full set of primitive equations to calculate the motion of water and the transport of heat and salt. The K-profile parameterization (KPP) was used as turbulence closure scheme. The model's western boundary opens into the Skagerrak and connects the Baltic Sea to the North Sea. The maximum depth was set at 264 meters. A more detailed description of the setup can be found in (gröger2022?).

### 3.4 Neural network hyper parameters

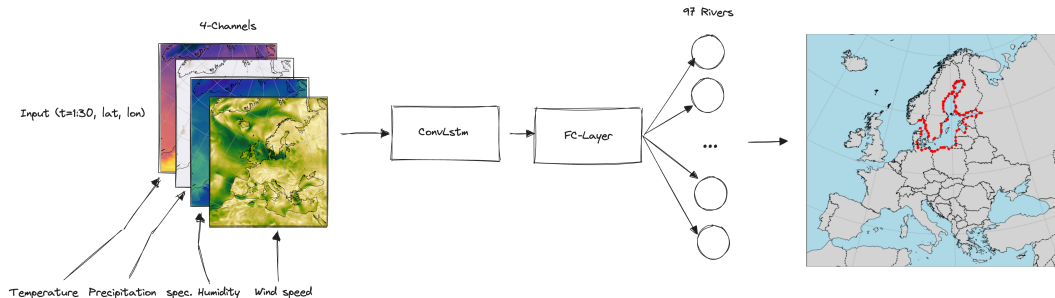


Figure 3: Schematic structure of the ConvLSTM implementation for river runoff forecasting.

For the computation we use the following set of hyper parameters:

Table 1: Hyperparameters

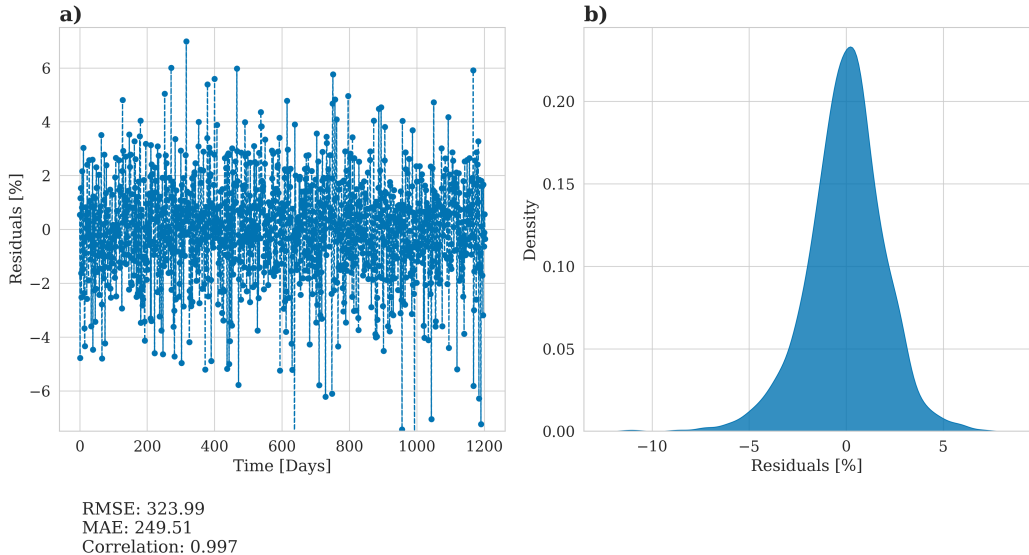
Parameter name	Parameter size
Channel size	4
Num. hidden layer	9
Num. timesteps	30
Conv. Kernelsize	(7,7)
Num. ConvLSTM layers	1
Batch size	50
Learning Rate	1e-3 with CosineAnnealing

As input the model receives  $N_\tau = 30$  days of atmospheric surface fields temperature  $T$ , precipitation  $P$ , specific humidity  $Q$  and wind speed  $W$ , with a daily resolution to predict the river runoff  $\bar{R}$ . The choice of atmospheric fields was based on the implemented river runoff calculation in the atmospheric model COSMO-CLM which uses these atmospheric fields to calculate an river runoff estimate.

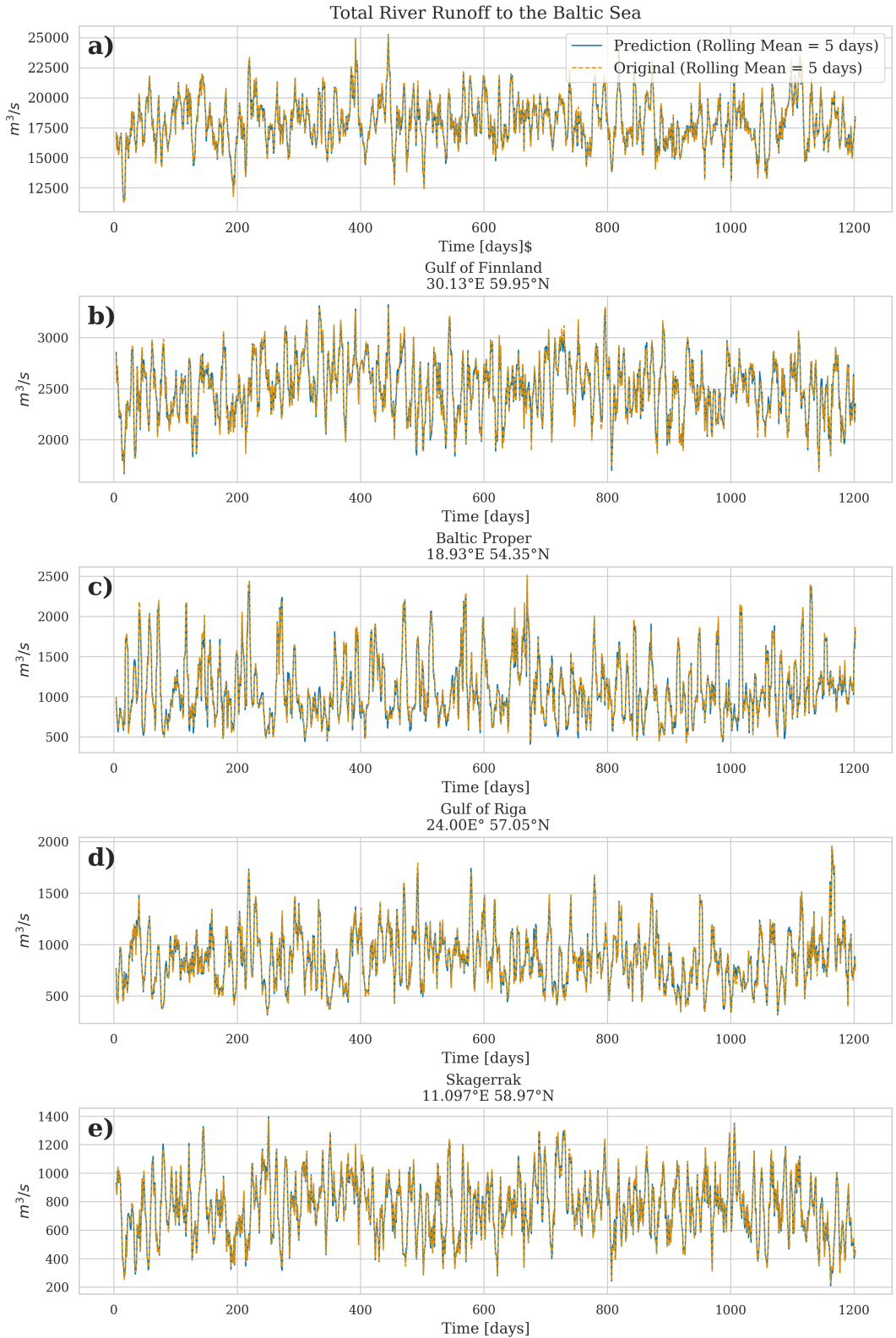
248 **4 Results**

249 The model was trained with daily data for the period 1979 to 2011, as this period  
 250 represents the only period of E-HYPE without further bias correction applied to the  
 251 runoff to match observations. The data was divided into randomly chosen splits of  
 252 80% training data, 10% validation data to evaluate the performance of the model  
 253 during training, and 10% training data which is finally used to evaluate the perfor-  
 254 mance of the model after training. The model was trained for 400 epochs and the  
 255 model weights with the lowest mean squared error during training have been stored.

256 The accuracy of the model is displayed in Figure ?@fig-statistical-evaluationNN.  
 257 As mention above for evaluation, the test dataset was utilized. The left panel panel  
 258 (Figure ?@fig-statistical-evaluationNN a) illustrates the relative prediction error  
 259 in relation to the original E-HYPE data, indicating that, on daily timescales, the  
 260 model can predict river runoff with an accuracy of  $\pm 5\%$ . The overall correlation is  
 261 0.997 with the resulting error metrics yielding a RMSE of  $323.99 \text{ m}^3/\text{s}$  and MAE  
 262 of  $249.51 \text{ m}^3/\text{s}$ . While the model's performance is satisfactory, the discrepancies  
 263 between the actual values and the predictions could partly be attributed to the use  
 264 of a different atmospheric dataset than the one originally used to drive the E-HYPE  
 265 model. However, by applying a rolling mean with a 5-day window, the prediction  
 266 error is reduced to less than 1%, which is acceptable for the purposes of climate  
 267 modeling. Lastly, the right panel demonstrates that the distribution of residuals  
 268 follows a Gaussian shape, suggesting that our model does not exhibit bias by system-  
 269 atically over or underestimating river runoff values.



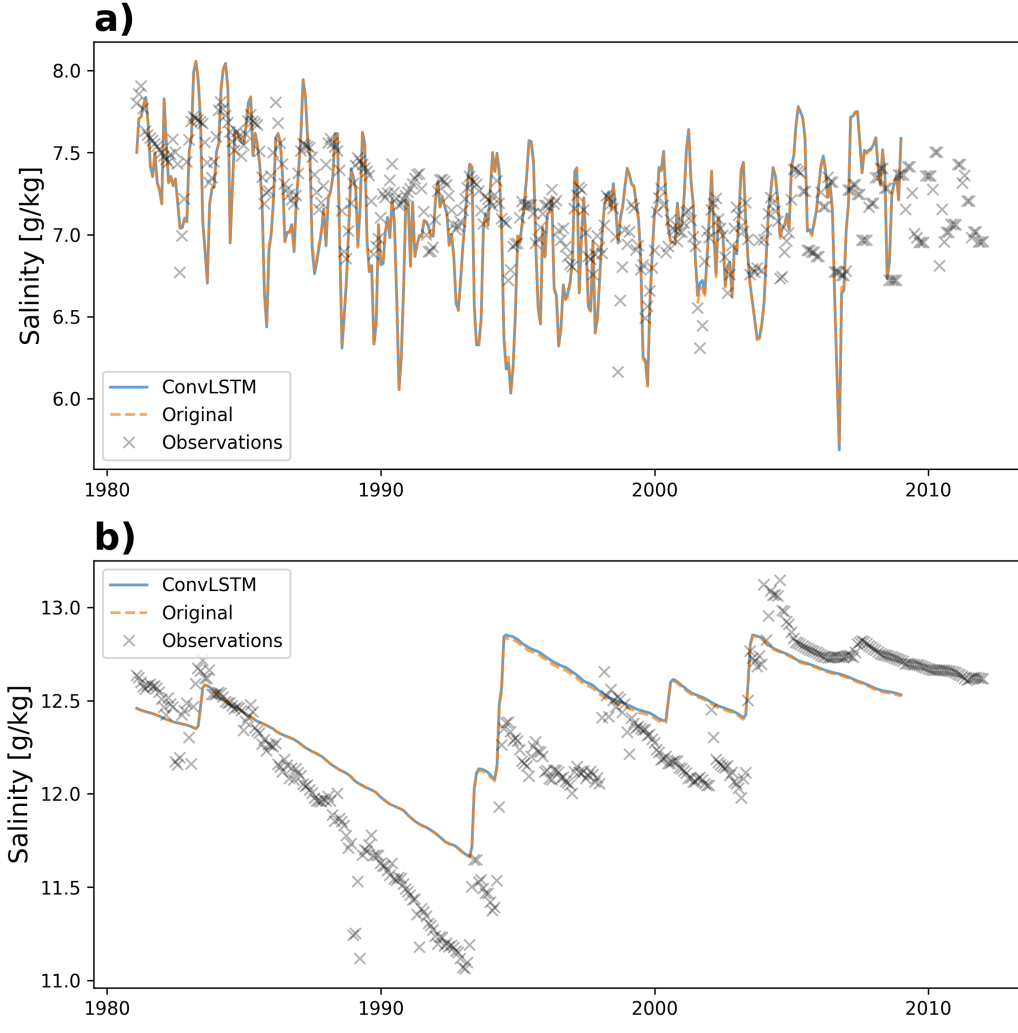
271 In the following we will now address the overall performance of the total river  
 272 runoff while also zooming in on the four largest rivers entering the Baltic Sea. @fig-  
 273 PerformanceNeuralNetworkRunoff shows the predicted and the original river runoff  
 274 using the test dataset. The predicted total river runoff for the Baltic Sea is closely  
 275 matching the original data (@fig-PerformanceNeuralNetworkRunoff a). Zooming in  
 276 on the largest individual rivers (@fig-PerformanceNeuralNetworkRunoff b-e) it can  
 277 be seen that that also the prediction of the individual rivers is close to the original  
 278 data.



279

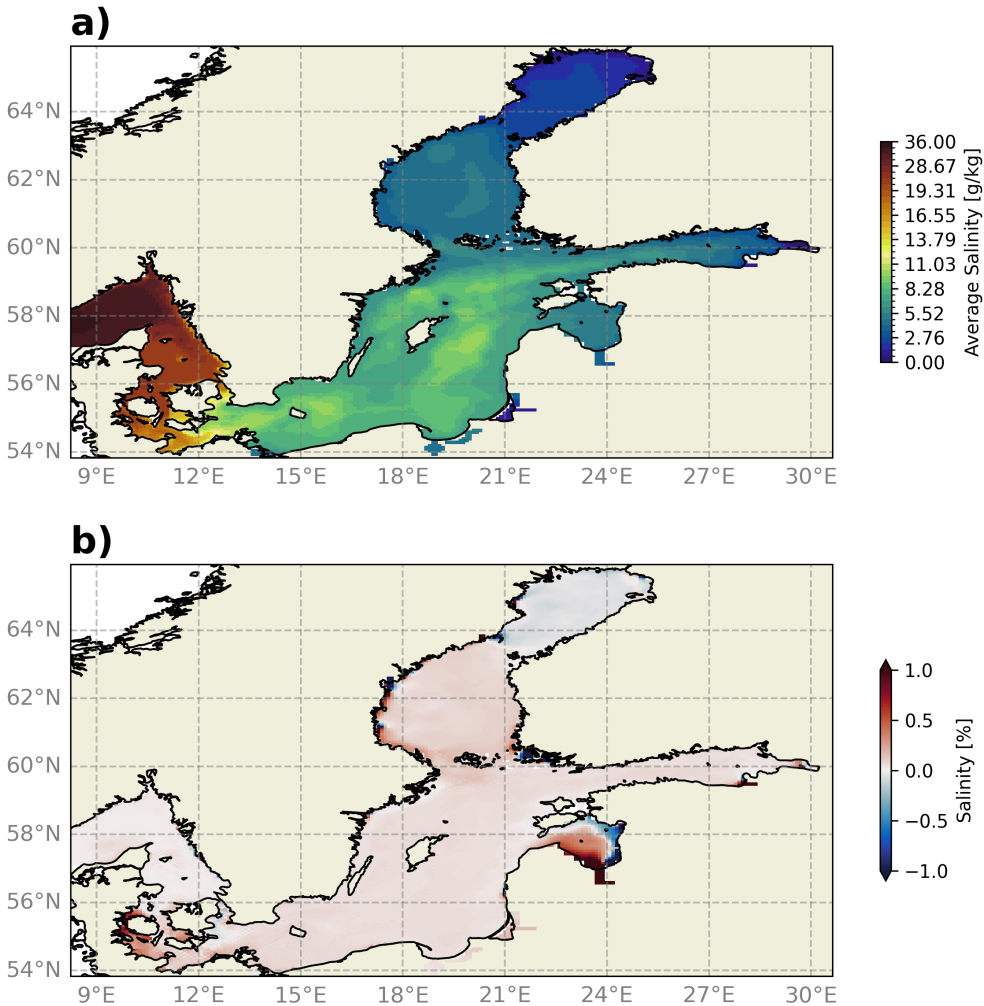
280 Lastly, we evaluated the performance of the runoff model by incorporating the pre-  
 281 dicted river runoff as runoff forcing into the ocean model MOM5. This provides a  
 282 robust validation of the runoff model against more complex real world conditions.  
 283 This allows us to ensure that the predictions accurately reflect the impact of the  
 284 river discharge on the ocean dynamics, validating the temporal and spatial variabil-

285 ity of the the river discharge. ?@fig-by15 shows the salinity comparison between  
 286 the original E-HYPE river runoff and the predicted river runoff at BY15 - a cen-  
 287 tral stations in the Baltic Sea. It can be seen that the model simulation using the  
 288 predicted river runoff by the ConvLSTM is closely mirroring the control simulation.  
 289 The upper panel (?@fig-by15 a) shows the surface salinity, representing the high-  
 290 frequency variations in the salinity, which is heavily affected by river runoff. The  
 291 lower panel (?@fig-by15 b) shows the bottom salinity which can be viewed as a  
 292 low-pass filter in the Baltic Sea, which is also closely mirrored by the ConvLSTM  
 293 predictions.



294

295 The final evaluation of the ConvLSTM model concentrates on the spatial accuracy  
 296 of river runoff predictions. Figure xxx a) shows the vertically averaged salinity for  
 297 the period 1981 to 2011 in the reference simulation. It highlights the strong horizon-  
 298 tal gradients and complex topographic features in the Baltic Sea, as evidenced by  
 299 salinity variations in deeper waters, captured by the vertical integration. Figure 4b  
 300 compares these results by showing the percentage difference in vertically averaged  
 301 salinity between the ConvLSTM simulation and the reference simulation. Overall,  
 302 the differences remain below 1%, except near a river mouth in the Gulf of Riga  
 303 (22-24°E, 56.5-58.5°N for orientation), where the difference is approximately 1%.



304

## 305 5 Discussion

306 With the increasing demand of decision makers for regional climate projections, that  
 307 allow to quantify regional climate change impacts, the availability of precise hydro-  
 308 logical forecasting becomes invaluable. The quality of a projection for a coastal sea  
 309 such as the Baltic Sea is too large parts based on the quality of the hyrdological con-  
 310 ditions. In this work we analyze the implementation of a ConvLSTM networks for  
 311 predicting river runoff, highlighting its potential to enhance river runoff forecasting  
 312 across different coastal seas. Given the unique hydrological characteristics of the  
 313 Baltic Sea, largely influenced by its limited connection to the open ocean and signifi-  
 314 cant freshwater input from surrounding rivers, the region presents a critical case for  
 315 the application of sophisticated forecasting models.

316 The transition from traditional hydrological models to machine learning approaches,  
 317 such as the ConvLSTM model, offers significant advantages. The ConvLSTM can be  
 318 seamlessly integrated into regional climate models, allowing for the real-time compu-  
 319 tation of river runoff while performing climate projections. While the initial training  
 320 of the model requires substantial computational resources, it remains less intensive  
 321 than running comprehensive hydrological models. Furthermore, once trained, the  
 322 ConvLSTM model is computationally efficient during inference, ensuring enhanced  
 323 forecasting capabilities without significantly increasing computational demands.

324 While the ConvLSTM represents an advancement for the climate community, given  
 325 that running and tuning traditional hydrological models demands extensive exper-  
 326 tise, models like E-HYPE maintain an essential role. They provide a comprehensive  
 327 dataset that helps to train our ConvLSTM model effectively. This robust training  
 328 enables the machine learning models to achieve highly accurate predictive weights.  
 329 Thus, rather than rendering traditional methods obsolete, the integration of machine  
 330 learning models builds upon and enhances the foundational data provided by them.

331 The robust performance of the ConvLSTM model in simulating river runoff and  
 332 its possible effective integration into regional climate models pave the way for a  
 333 multitude of new storyline simulations. Hence, we can now explore various “what-  
 334 if” scenarios more reliably, under the assumption that the model weights attained  
 335 during training are robust.

336 In summary, we showed that the ConvLSTM model demonstrated robust perfor-  
 337 mance in forecasting river runoff across 97 rivers entering the Baltic Sea. Trained  
 338 on data from 1979 to 2011, the model achieved an impressive daily prediction accu-  
 339 racy of  $\pm 5\%$ . This capability to generate accurate and detailed simulations enables  
 340 to examine the potential impacts of different climate scenarios. Such precision in  
 341 forecasting and scenario testing is crucial for crafting effective water resource man-  
 342 agement strategies and adapting to the changing climate.

343 Ultimately, the integration of ConvLSTM into regional climate models represents a  
 344 significant step forward in our ability to understand and predict the complex dynam-  
 345 ics of river systems and their impact on regional climate systems.

## 346 **6 Acknowledgments**

347 The research presented in this study is part of the Baltic Earth program (Earth  
 348 System Science for the Baltic Sea region, see <https://www.baltic.earth>.

## 349 **References**

- 350 Fang, W., Huang, S., Ren, K., Huang, Q., Huang, G., Cheng, G., & Li, K. (2019).  
 351 Examining the applicability of different sampling techniques in the development  
 352 of decomposition-based streamflow forecasting models. *Journal of Hydrology*, 568,  
 353 534–550. <https://doi.org/10.1016/j.jhydrol.2018.11.020>  
 354 Hagemann, S., Stacke, T., & Ho-Hagemann, H. T. M. (2020). High Resolution Dis-  
 355 charge Simulations Over Europe and the Baltic Sea Catchment. *Frontiers in*  
 356 *Earth Science*, 8. <https://doi.org/10.3389/feart.2020.00012>  
 357 SHI, X., Chen, Z., Wang, H., Yeung, D.-Y., Wong, W., & WOO, W. (2015). Con-  
 358 volutional LSTM Network: A Machine Learning Approach for Precipitation  
 359 Nowcasting. In *Advances in Neural Information Processing Systems* (Vol. 28).  
 360 Curran Associates, Inc. Retrieved from <https://proceedings.neurips.cc/paper/2015/hash/07563a3fe3bbe7e3ba84431ad9d055af-Abstract.html>  
 361 Tan, Q.-F., Lei, X.-H., Wang, X., Wang, H., Wen, X., Ji, Y., & Kang, A.-Q. (2018).  
 362 An adaptive middle and long-term runoff forecast model using EEMD-ANN hy-  
 363 brid approach. *Journal of Hydrology*, 567, 767–780. <https://doi.org/10.1016/j.jhydrol.2018.01.015>